

# A dimensionally-heterogeneous closed-loop model for the cardiovascular system

P.J. Blanco<sup>a,b,\*</sup>, R.A. Feijóo<sup>a,b</sup>

<sup>a</sup>*Laboratório Nacional de Computação Científica, Av. Getúlio Vargas 333, Quitandinha, 25651-075, Petrópolis, Brazil, pjblanco@lncc.br, feij@lncc.br*

<sup>b</sup>*Instituto Nacional de Ciência e Tecnologia em Medicina Assistida por Computação Científica, Av. Getúlio Vargas 333, Quitandinha, 25651-075, Petrópolis, Brazil*

---

## Abstract

In the present work a computational model of the entire cardiovascular system is developed using heterogeneous mathematical representations. This model stands for the integration of different levels of detail for the blood circulation. Indeed, the arterial tree is described by a one dimensional model in order to simulate the propagation phenomena that takes place at the larger arterial vessels. The inflow and outflow locations of this 1D model are coupled with proper lumped parameter descriptions (0D model) of the remainder part of the circulatory system, closing the loop. For the four cardiac valves we employ a valve model allowing for stenoses and regurgitation phenomena during the valve closing. In addition, full 3D geometrical models of arterial districts are embedded in this closed-loop circuit to model the local blood flow in specific vessels. An example of application involving the effect of aortic insufficiency on the local hemodynamics of a cerebral aneurism is provided as a motivation to study scenarios seen in certain patients suffering from infective endocarditis and mycotic aneurisms. The need for incorporating homeostatic control mechanisms is also discussed.

*Key words:* closed-loop system, heterogeneous models, systemic circulation, cardiac circulation, valve models, integrative model

---

\*Corresponding author.

Email addresses: pjblanco@lncc.br (P.J. Blanco), feij@lncc.br (R.A. Feijóo)

## 1. Introduction

The structural and functional behavior of the cardiovascular system can be considered as the result of the interplay among different levels of detail for describing the blood circulation. The integration of these levels of detail is mandatory in order to gain insight about the way in which local and global phenomena are inter-related.

In the context of the modeling the hemodynamic aspects of the cardiovascular system, and particularly in the present work, we identify the following levels of detail (also called levels of integration): (i) the hemodynamics of large arteries, (ii) the local circulation in specific vessels, (iii) the peripheral circulation, (iv) the venous circulation and (v) the cardiac/pulmonary circulation. Such levels of circulation sometimes refer to a certain geometrical scale (for instance the blood flow in large arteries, or in specific districts), and sometimes refer to a given vascular entity (the heart, or a given peripheral bed).

In the literature there have been several approaches to integrate different levels of circulation in the sense introduced in the previous paragraphs. Mostly, models based on lumped representations were employed to accomplish this task [21, 23, 24, 32, 36, 37], incorporating 0D models to simulate flow in the larger arteries, veins and cardiac circulation. As well, distributed models for simulating the blood flow in compliant vessels has been an exhaustive area of research through the last decades [1, 2, 22, 29, 33, 38, 39, 43]. More recently, in [26], 1D models of the arterial circulation have been coupled to 0D models of the venous-cardiac-pulmonary circulation to study the influence of arterial stenoses on the wave propagation. Particularly, the 1D model employed in [26] was taken from [38] and is comprised of 55 arterial segments and a 0D lumped representation for the peripheral/venous/pulmonary and cardiac circulations. In turn, valves are modeled using an ideal model of a diode, not allowing for backflow to occur. This last point has been addressed in [21], in which phenomenological models of the cardiac valves are proposed to model more accurately the opening and closing phases of the valves, being capable of modeling certain pathological conditions like valve regurgitation and stenosis. In this last work these valve models are coupled to a purely 0D representation of the closed-loop cardiovascular system.

In the field of modeling blood flow in specific vessels, several works have dealt with the use of heterogeneous representations in order to couple local and global hemodynamics phenomena. This has been mostly carried out

using 3D and 1D (or 0D) models to couple blood flow in complex arterial geometries with either full or partial geometrical descriptions for the systemic dynamics [4, 5, 6, 11, 12, 18, 27, 40, 42].

In the context introduced in the previous paragraphs, the present work presents a computational model of the entire cardiovascular system borrowing the most important features of the different models available in the literature. Thus, the model introduced here has more descriptive capabilities than the models currently available in the literature. Indeed, it allows to account for specific vessels, systemic arteries, peripheral circulation, systemic veins, pulmonary and heart circulation and complex valve functioning. Rather than multiscale modeling of the cardiovascular system in this case we refer to *integrative modeling* of the cardiovascular system. In the present approach, the arterial tree is described by a one dimensional model with 128 arterial segments, following [2], in order to simulate the propagation phenomena in the larger arterial vessels. The inflow and outflow locations of this 1D model are coupled with proper lumped parameter descriptions (0D model) of the remainder part of the circulatory system, closing the network. At each outflow point we incorporate the peripheral circulation in arterioles and capillaries by using 0D three-component Windkessel models, following [38]. In turn, the whole peripheral circulation converges to the venous system through the upper and lower parts of the body (using the ideas proposed in [26]). These two main compartments are represented using lumped models for the venules, veins and cavas (inferior and superior). The right and left heart circulation, as well as the pulmonary circulation are also modeled by means of 0D models. Particularly we point out the modeling of the four heart valves, which is carried out by using a non-linear model which allows for the regurgitation phase during the valve closing, following [21]. Finally, the 0D model of the left ventricle is coupled with the inflow boundary in the 1D model, closing the cardiovascular loop. The entire 0D model which performs the coupling between the outflow and inflow points in the arterial tree consists of 14 compartments. Moreover, following [4, 5, 6], we consider the existence of 3D models accounting for all the complexity of three-dimensional blood flow in specific vessels of interest.

This work is organized as follows. Section 2 presents all the mathematical representations used in this work for the different levels of circulation. Section 3 provides the data upon which our model is set up. In Section 4 the model is employed to simulate different cardiovascular scenarios involving such heterogeneous models. The final remarks are given in Section 5.

## 2. Mathematical models for the vascular entities

### 2.1. 1D model for the systemic arteries

The blood flow in the systemic arteries is modeled using a 1D model derived from the Navier-Stokes equations by introducing suitable assumptions. This procedure yields, for a generic 1D segment  $\mathcal{I}$ , the following (see [15] for its derivation)

$$\begin{cases} \frac{\partial Q}{\partial t} + \frac{\partial}{\partial x} \left( \beta \frac{Q^2}{A} \right) = -\frac{A}{\rho} \frac{\partial P}{\partial x} - \frac{\pi D}{\rho} \tau_o & \text{in } \mathcal{I}, \\ \frac{\partial A}{\partial t} + \frac{\partial Q}{\partial x} = 0 & \text{in } \mathcal{I}, \end{cases} \quad (1)$$

where  $\tau_o = f_r \frac{\rho \tilde{u} |\tilde{u}|}{8}$ ,  $Q = \tilde{u} A$ ,  $A$  is the cross sectional area of the artery ( $D$  its diameter),  $\tilde{u}$  the mean value of the axial velocity,  $x$  the axial coordinate,  $P$  the mean pressure,  $\rho$  the blood density,  $\tau_o$  the viscous shear stress acting on the arterial wall,  $f_r$  a Darcy friction factor (in this work a fully developed parabolic velocity profile is considered) and  $\beta$  is the momentum correction factor ( $\beta = 1$  is considered here).

The system is closed by introducing a constitutive law which establishes a relation between the pressure and the cross sectional area. Here a non-linear visco-elastic model [19, 20] is used

$$P = P_o + \frac{h_o E_e}{R_o} \varepsilon + \frac{K h_o}{R_o} \dot{\varepsilon} \quad \text{in } \mathcal{I}, \quad (2)$$

where  $\varepsilon = \sqrt{\frac{A}{A_o}} - 1$ ,  $R$  is the radius of the artery,  $E_e$  is the effective Young modulus of the elastin,  $E_c$  is the effective Young modulus of the collagen fibers,  $K$  is the effective viscosity of the wall,  $h$  is the thickness of the arterial wall and the subscript ‘o’ denotes quantities evaluated at the reference pressure  $P_o$ .

### 2.2. 0D model for the arterioles and capillaries

The peripheral circulation is represented through Windkessel models [36, 38]. The Windkessel behavior is determined by a resistance  $R_c$  to represent the capillaries, in series with the parallel of a resistance  $R_a$  and a capacitor  $C_a$  to model the arterioles. Here,  $P_i$  and  $P_o$  are the pressures at the input and output of the compartment, respectively,  $Q_i$  and  $Q_o$  are the blood inflow and outflow, respectively. The balance equations for this model are the following

$$\begin{cases} \frac{dQ_i}{dt} = \frac{1}{R_c R_a C_a} \left[ R_a C_a \frac{d}{dt} (P_i - P_o) + (P_i - P_o) - (R_c + R_a) Q_i \right], \\ Q_i = Q_o. \end{cases} \quad (3)$$

The Windkessel element plays the role of an interface between arterial and venous systems. Thus the  $P_i$  is the pressure from the arterial side (at the input of the compartment) while  $P_o$  is the pressure from the venous side (at the output of the compartment), more precisely at the venules.

### 2.3. 0D model of the venous and pulmonary circulation

The models to simulate the blood flow through the venules, veins, superior and inferior vena cava and also the pulmonary arteries and pulmonary veins are formulated in terms of an  $R-L-C$  analog electric circuit. A single compartment is characterized by its resistance ( $R$ ), inertance ( $L$ ) and compliance ( $C$ ). Further,  $P_i$  ( $Q_i$ ) and  $P_o$  ( $Q_o$ ) are the pressures (flow rates) at the input and output of the compartment, respectively,  $P_{ex}$  is the external pressure which also could be a function of time. The governing equations associated to this generic compartment are given by

$$\begin{cases} L \frac{dQ_o}{dt} + RQ_o = P_i - P_o, \\ C \frac{d}{dt}(P_i - P_{ex}) = Q_i - Q_o, \end{cases} \quad (4)$$

for the case when  $C$  is constant. In our simulations we specified the external pressure  $P_{ex} = 0$ .

### 2.4. 0D model for the heart and valves

The whole cardiac circulation is divided into two halves. Each half consists of two chambers and two valves. We divide the presentation here in order to separate the balance equations at the cardiac chambers and at the heart valves. In the present work, the model for the cardiac chambers and the notation follows [26].

#### 2.4.1. Elastance model for the cardiac chambers

Elastance-based modeling of the heart has been adopted in this study to describe each of the four cardiac chambers. Thus the pressure in each cardiac chamber, denoted by  $P_i$ , is related to the chamber volume  $V_{ch}$  as

$$P_i - P_{ex} = (E_A e(t) + E_B)(V_{ch} - V_{0,ch}) + \alpha_{ch} |P_i| \frac{dV_{ch}}{dt}, \quad (5)$$

where  $V_{0,ch}$  refers to the dead volume of the chamber and  $\alpha_{ch}$  reflects the fact that in the pressure-volume relation follows a viscoelastic behavior. In turn,

$E_A$  and  $E_B$  are the amplitude and baseline values of the elastance, and  $e(t)$  is a normalized time-varying function of the elastance, which for ventricles is

$$e_v(t) = \begin{cases} \frac{1}{2} \left[ 1 - \cos \left( \pi \frac{t}{T_{vc}} \right) \right] & 0 \leq t \leq T_{vc} \\ \frac{1}{2} \left[ 1 + \cos \left( \pi \frac{(t-T_{vc})}{T_{vr}} \right) \right] & T_{vc} < t \leq T_{vc} + T_{vr} \\ 0 & T_{vc} + T_{vr} < t \leq T \end{cases} \quad (6)$$

and for atria is

$$e_a(t) = \begin{cases} \frac{1}{2} \left[ 1 + \cos \left( \pi \frac{(t-T_{tar})}{T_{ar}} \right) \right] & 0 \leq t \leq t_{ar} + T_{ar} - T \\ 0 & t_{ar} + T_{arp} - T < t \leq t_{ac} \\ \frac{1}{2} \left[ 1 - \cos \left( \pi \frac{(t-t_{ac})}{T_{ac}} \right) \right] & t_{ac} < t \leq t_{ac} + T_{ac} \\ \frac{1}{2} \left[ 1 + \cos \left( \pi \frac{(t-t_{tar})}{T_{ar}} \right) \right] & t_{ac} + T_{ac} < t \leq T \end{cases} \quad (7)$$

Here, the subscript  $v$  denotes the ventricles, and  $a$  the atria,  $T$  is the duration of a cardiac cycle,  $T_{vc}$ ,  $T_{ac}$ ,  $T_{vr}$  and  $T_{ar}$  refer to the durations of ventricular/atrial contraction/relaxation, and  $t_{ac}$ ,  $t_{ar}$  the times when the atria begin to contract and relax, respectively.

Finally, the volume is related to the inflow and outflow as usual

$$\frac{dV_{ch}}{dt} = Q_i - Q_o. \quad (8)$$

#### 2.4.2. Non-ideal diode model for the heart valves

The momentum balance in each heart valve is such that we take into account the possibility of inverted flow when the valve closes. The model employed has been partially inspired in the valve model presented in [21]. The governing equation is the following

$$L \frac{dQ_o}{dt} + RQ_o + B|Q_o|Q_o = \Xi(P_i - P_o), \quad (9)$$

where  $L$  is the inertance of the fluid,  $R$  is the viscous resistance,  $B$  accounts for the flow separation phenomenon and  $P_i$  and  $P_o$  are the input and output pressure values in the compartment. The non-binary state of the valve is considered through the coefficient  $\Xi$ . This coefficient simulates the behavior of the orifice of the valve, and is a function of the opening angle of the valve, denoted by  $\theta$ , as follows

$$\Xi = \frac{(1 - \cos \theta)^4}{(1 - \cos \theta_{max})^4}. \quad (10)$$

where  $\theta_{max}$  is the maximum angle the valve is able to open. An heuristic angular momentum balance equation for  $\theta$  is used here (see [21] for the derivation and details) as follows

$$I \frac{d^2\theta}{dt^2} + k_F \frac{d\theta}{dt} = k_P(P_i - P_o) + k_Q Q_o \cos \theta + \begin{cases} k_V Q_o \sin(2\theta) & \text{if } P_i \geq P_o \\ 0 & \text{if } P_i < P_o \end{cases}, \quad (11)$$

where  $I$  is the momentum of inertia of the valve. The solution of this balance equation is constrained to

$$\theta = \begin{cases} \theta_{min} & \text{if } \theta < \theta_{min}, \\ \theta_{max} & \text{if } \theta > \theta_{max}. \end{cases} \quad (12)$$

In this way, a valve can undergo malfunctioning in either of two distinct ways (or combination of them). These are *stenosis* if the valve is narrowed (reduced value of  $\theta_{max}$ ), and *incompetence* or *insufficiency* when the valve is leaky and fails to prevent prominent backward flow (increased value of  $\theta_{min}$ ).

### 2.5. 3D model for specific vessels

The Navier-Stokes equations in moving domains (ALE formulation) are employed for describing the blood flow in specific arterial vessels. Then, the equations for a domain  $\Omega$  are

$$\begin{cases} \rho \frac{\partial \mathbf{u}}{\partial t} + \rho (\mathbf{u} - \mathbf{v}) \nabla \mathbf{u} - \mu \Delta \mathbf{u} + \nabla P = \mathbf{f} & \text{in } \Omega, \\ \operatorname{div} \mathbf{u} = 0 & \text{in } \Omega, \end{cases} \quad (13)$$

where  $\mathbf{u}$  is the fluid velocity,  $\mathbf{v}$  is the velocity of the frame of reference,  $P$  is the pressure field,  $\mathbf{f}$  is the volume body force and  $\rho$  and  $\mu$  are density and viscosity, respectively. This set of equations must be provided with proper boundary conditions and a proper constitutive relation relating the displacement of the arterial wall with the pressure (structural model). As in our previous works [4, 40], we choose an independent rings wall model consistent with that used for the 1D model, that is ( $\partial\Omega_w$  stands for the arterial wall)

$$\begin{cases} P - P_o = \frac{E_e h_o}{R_o^2} \delta + \frac{K h_o}{R_o^2} \frac{d\delta}{dt} & \text{on } \partial\Omega_w \\ \mathbf{w} = \delta \mathbf{n} & \text{on } \partial\Omega_w \\ \mathbf{v} = \frac{\partial \mathbf{w}}{\partial t} & \text{in } \Omega \end{cases} \quad (14)$$

where  $\delta$  is the displacement of the surface points in the direction of the normal vector  $\mathbf{n}$ ,  $\mathbf{w}$  is the displacement vector for the deformable domain with respect to its reference configuration, which is extended to the interior of the domain by solving the problem  $\Delta \mathbf{w} = 0$  in  $\Omega$  with Dirichlet boundary condition given by (14)<sub>2</sub>. It is evident the analogy between the equation (14)<sub>1</sub> to that given in (2)<sub>1</sub> (without collagen) for the 1D model.

Other constitutive behaviors for the blood are also incorporated in the model, giving rise to an equation similar to (13) but now valid for non-Newtonian fluids. In the present work we employ the Casson model for which the blood viscosity is given by

$$\mu = \left( \sqrt{\mu_o} + \sqrt{\frac{\tau_y}{\epsilon}} \right)^2, \quad (15)$$

where  $\mu_o$  is the asymptotic viscosity,  $\tau_y$  is the yield stress at which the fluid starts to flow and the shear rate is given by  $\epsilon = \sqrt{2(\nabla \mathbf{u})^s \cdot (\nabla \mathbf{u})^s}$ , being  $(\cdot)^s$  the symmetric component of the second order tensor  $(\cdot)$ .

Finally, when the 3D model is coupled to a 1D model the following coupling equations are incorporated

$$\begin{cases} Q_i = \int_{\Gamma_i} \mathbf{u} \cdot \mathbf{n} d\Gamma_i & \text{at } \Gamma_i \quad i = 1, \dots, N_{cf}, \\ P_i = ((P\mathbf{I} - \mu(\nabla \mathbf{u})^s)\mathbf{n})|_{\Gamma_i} & \text{at } \Gamma_i \quad i = 1, \dots, N_{cf}, \end{cases} \quad (16)$$

where  $(Q_i, P_i)$  are the quantities shared with the 1D model which is coupled to the 3D model at interface  $\Gamma_i$ ,  $i = 1, \dots, N_{cf}$ , being  $N_{cf}$  the total number of coupling interfaces in that 3D model.

### 2.6. Entire coupled model

The entire model is schematically shown in Figure 1, and the corresponding notation is given in Table 1. In this table  $N_{sa}$  denotes the total number of systemic arteries employed and  $N_{wlb}$  and  $N_{wub}$  are the number of Windkessel models pertaining to the lower and upper parts of the body, respectively, with  $N_w = N_{wlb} + N_{wub}$  the total number of Windkessel elements. There, a summary of the equations for each model is presented. The notation of Table 1 is used to identify the material parameters provided in Section 3.

## 3. Physiological data

In this section we collect all the data used in setting the 1D-0D closed-loop model of the cardiovascular system for the sake of completeness. These

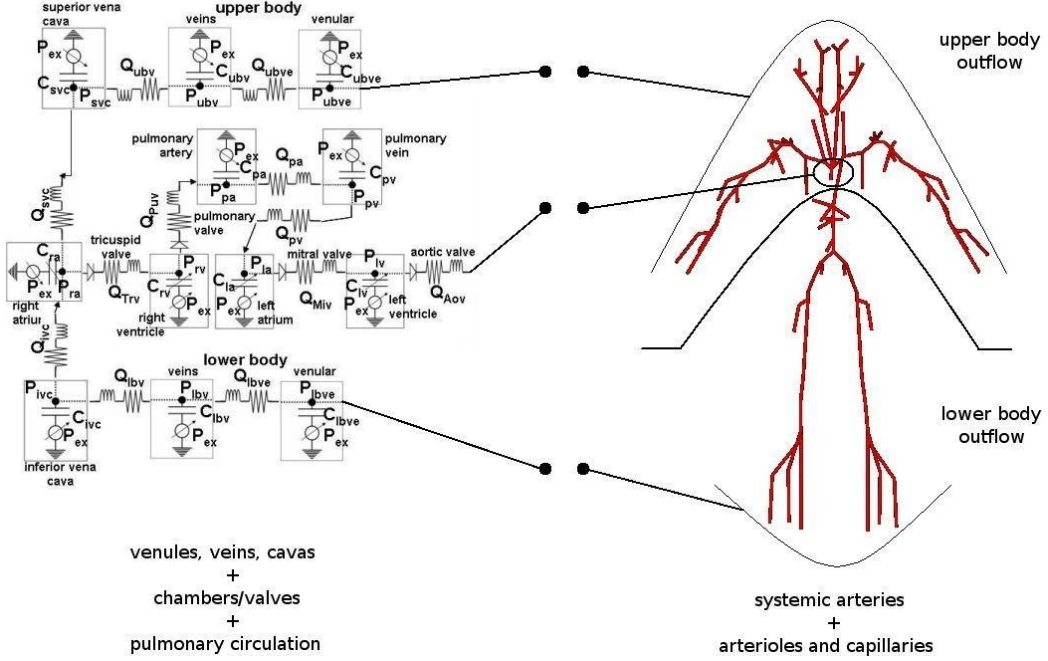


Figure 1: Entire closed-loop model of the cardiovascular system.

notation	vascular entity	governing equations
sa,m:	systemic arteries, $m = 1, \dots, N_{sa}$	(1) - (2)
wlb,k:	lower body Windkessel models, $k = 1, \dots, N_{wlb}$	(3)
wub,k:	upper body Windkessel models, $k = 1, \dots, N_{wub}$	(3)
lbve:	lower body venule	(4)
lbv:	lower body veins	(4)
ubve:	upper body venule	(4)
ubv:	upper body veins	(4)
ivc:	inferior vena cava	(4)
svc:	superior vena cava	(4)
pa:	pulmonary artery	(4)
pv:	pulmonary vein	(4)
ra:	right atria	(5) - (7) - (8)
rv:	right ventricle	(5) - (6) - (8)
la:	left atria	(5) - (7) - (8)
lv:	left ventricle	(5) - (6) - (8)
Trv:	tricuspid valve	(9) - (11)
Puv:	pulmonary valve	(9) - (11)
Miv:	mitral valve	(9) - (11)
Aov:	aortic valve	(9) - (11)
3D:	three-dimensional model	(13) - (14) - (16)

Table 1: Glossary of the terms used in Figure 1 and summary of the models.

parameters have been retrieved from or estimated based on the data reported in [2, 13, 14, 21, 24, 25, 26, 28, 31, 38, 41].

### 3.1. Larger arteries

The values for the density and the viscosity of the blood are  $\rho = 1.04 \text{ g/cm}^3$  and  $\mu = 0.04 \text{ dyn s/cm}^2$ , respectively. The parameters used in the 1D model of the arterial tree have been adapted from [2], and are given in Table 2. The viscoelasticity coefficient was taken so that it renders a viscoelastic angle  $\phi = \arctan\left(\frac{\omega K}{E_e}\right) = 10^\circ$ , for which we consider a characteristic frequency  $\omega = \frac{2\pi}{T_K}$ , with  $T_K = 0.4 \text{ s}$ .

### 3.2. Arterioles and Capillaries

The parameters that characterize the behavior of the arterioles and capillaries through the Windkessel element have been computed according to the guidelines provided in [38], and are given in Table 3.

### 3.3. Venules, veins and inferior and superior vena cava

The elements of the 0D model for the venous system are calibrated using the data provided in Table 4, mostly taken from [26].

### 3.4. Right and left hearts

The data for the elastance model of the right and left hearts as well as the data needed by the model for the valves are provided in Table 5 and Table 6, and are based on [21, 26]. The cardiac cycle is defined with a period  $T = 1 \text{ s}$ .

### 3.5. Pulmonary arteries and veins

The data for the 0D models that represent both the pulmonary arteries and veins are given in Table 7.

### 3.6. Specific vessels

The geometrical data corresponding to set up three-dimensional models of arterial vessels is obtained either by resorting to a standard geometry or to medical images. This will be clear in each specific example. In the case of patient-specific vessels, the extraction of the anatomical structures is done following standard steps for the segmentation of the corresponding medical images.

Regarding mechanical parameters ( $E_e$  and  $K$  in equation (14)) the arterial wall parameters in the 3D model match those pertaining to the 1D model in

Segment	Description	$l$ [cm]	$R_o$ [cm]	$h_o$ [cm]	$E_e$ [dyn/cm $^2$ ]	$K$ [dyn s/cm $^2$ ]
1	Ascending aorta	4.0	1.45	0.163	4000000	44000
2	Aortic arch	2.0	1.12	0.132	4000000	44000
5	Aortic arch	3.9	1.07	0.127	4000000	44000
11	Thoracic aorta	5.2	1.00	0.120	4000000	44000
21	Thoracic aorta	5.2	0.95	0.116	4000000	44000
34	Thoracic aorta	5.2	0.95	0.116	4000000	44000
50	Abdominal aorta	5.3	0.87	0.108	4000000	44000
65	Abdominal aorta	5.3	0.57	0.080	4000000	44000
75	Abdominal aorta	5.3	0.57	0.080	4000000	44000
49	Coeliac artery	1.0	0.39	0.064	4000000	44000
61	Gastric artery	7.1	0.18	0.045	4000000	44000
62	Splenic artery	6.3	0.28	0.054	4000000	44000
63	Hepatic artery	6.6	0.22	0.049	4000000	44000
64	Renal artery	3.2	0.26	0.053	4000000	44000
66	Superior mesenteric	5.9	0.43	0.069	4000000	44000
67	Gastric artery	3.2	0.26	0.053	4000000	44000
83	Inferior mesenteric	5.0	0.16	0.043	4000000	44000
4	L. common carotid	8.9	0.37	0.063	4000000	44000
10	L. common carotid	8.9	0.37	0.063	4000000	44000
20	L. common carotid	3.1	0.37	0.063	4000000	44000
12	R. common carotid	8.9	0.37	0.063	4000000	44000
22	R. common carotid	8.9	0.37	0.063	4000000	44000
3	L. subclavian artery	3.4	0.42	0.067	4000000	44000
6	Brachiocephalic artery	3.4	0.62	0.086	4000000	44000
82,84	Common iliac	5.8	0.52	0.076	4000000	44000
89,92	External iliac	8.3	0.29	0.055	4000000	44000
90,91	Internal iliac	5.0	0.20	0.040	16000000	178000
98,99	External iliac	6.1	0.27	0.053	4000000	44000
104,107	Femoral artery	12.7	0.24	0.050	8000000	89000
105,106	Profundis artery	12.6	0.23	0.049	16000000	178000
109,110	Femoral artery	12.7	0.24	0.050	8000000	89000
111,112	Popliteal artery	9.4	0.20	0.047	8000000	89000
113,114	Popliteal artery	9.4	0.20	0.050	4000000	44000
115,118	Anterior tibial artery	2.5	0.13	0.039	16000000	178000
119,124	Anterior tibial artery	15.0	0.10	0.020	16000000	178000
125,128	Anterior tibial artery	15.0	0.10	0.020	16000000	178000
116,117	Posterior tibial artery	16.1	0.18	0.045	16000000	178000
121,122	Posterior tibial artery	16.1	0.18	0.045	16000000	178000
120,123	Peroneal artery	15.9	0.13	0.039	16000000	178000
126,127	Peroneal artery	15.9	0.13	0.019	16000000	178000

Table 2: Geometric and mechanical parameters of the arterial segments.

Segment	Description	$l$ [cm]	$R_o$ [cm]	$h_o$ [cm]	$E_e$ $\frac{\text{dyn}}{\text{cm}^2}$	$K$ $\frac{\text{dyn s}}{\text{cm}^2}$
31,37	Carotid (internal)	5.9	0.18	0.045	8000000	89000
32,36	External carotid	11.8	0.15	0.042	8000000	89000
33,35	Superior thyroid artery	4.0	0.07	0.020	8000000	89000
43,56	Lingual artery	3.0	0.10	0.030	8000000	89000
44,55	Internal carotid	5.9	0.13	0.039	8000000	89000
45,54	Facial artery	4.0	0.10	0.030	16000000	178000
46,53	Middle cerebral	3.0	0.06	0.020	16000000	178000
47,52	Cerebral artery	5.9	0.08	0.026	16000000	178000
48,51	Ophthalmic artery	3.0	0.07	0.020	16000000	178000
60,68	Internal carotid	5.9	0.08	0.026	16000000	178000
73,77	Superficial temporal	4.0	0.06	0.020	16000000	178000
74,76	Maxillary artery	5.0	0.07	0.020	16000000	178000
7,15	Internal mammary	15.0	0.10	0.030	8000000	89000
8,14	Subclavian artery	6.8	0.40	0.066	4000000	44000
9,13	Vertebral artery	14.8	0.19	0.045	8000000	89000
16,26	Costo-cervical artery	5.0	0.10	0.030	8000000	89000
17,25	Axillary artery	6.1	0.36	0.062	4000000	44000
18,24	Suprascapular	10.0	0.20	0.052	8000000	89000
19,23	Thyrocervical	5.0	0.10	0.030	8000000	89000
27,41	Thoraco-acromial	3.0	0.15	0.035	16000000	178000
28,40	Axillary artery	5.6	0.31	0.057	4000000	44000
29,39	Circumflex scapular	5.0	0.10	0.030	16000000	178000
30,38	Subscapular	8.0	0.15	0.035	16000000	178000
42,57	Brachial artery	6.3	0.28	0.055	4000000	44000
58,70	Profunda brachi	15.0	0.15	0.035	8000000	89000
59,69	Brachial artery	6.3	0.26	0.053	4000000	44000
71,79	Brachial artery	6.3	0.25	0.052	4000000	44000
72,78	Superior ulnar collateral	5.0	0.07	0.020	16000000	178000
80,86	Inferior ulnar collateral	5.0	0.06	0.020	16000000	178000
81,85	Brachial artery	4.6	0.24	0.050	4000000	44000
87,94	Ulnar artery	6.7	0.21	0.049	8000000	89000
88,93	Radial artery	11.7	0.16	0.043	8000000	89000
95,102	Ulnar artery	8.5	0.19	0.046	8000000	89000
96,101	Interossea artery	7.9	0.09	0.028	16000000	178000
97,100	Radial artery	11.7	0.16	0.043	8000000	89000
103,108	Ulnar artery	8.5	0.19	0.046	8000000	89000

Table 2: Geometric and mechanical parameters of the arterial segments.

Terminal	$R_c$	$R_a$	$C_a$
	$\frac{\text{dyn s}}{\text{cm}^2 \text{ml}}$	$\frac{\text{ml cm}^2}{\text{dyn}}$	
125,128	62781.6	251356	1.00E-006
126,127	31792.6	127400	1.00E-006
121,122	21693	86769.2	2.00E-006
105,106	12280.8	49008.4	4.00E-006
90,91	15724.8	62781.6	3.00E-006
83	31103.8	125104	2.00E-006
64	3971.8	15839.6	1.20E-005
66	3329.2	13314	1.40E-005
67	3971.8	15839.6	1.20E-005
61	23758	94918.6	2.00E-006
62	8608.6	34433	5.00E-006
63	6851.6	27431.6	7.00E-006
9,13	22037.4	88032	2.00E-006
7,15	89409.6	358092	1.00E-006
19,23	89409.6	358092	1.00E-006
18,24	20774.6	83326.6	2.00E-006
16,26	89409.6	358092	1.00E-006
30,38	84015.4	198562	1.00E-006
29,39	126252	506156	0.00E+000
27,41	84015.4	198562	1.00E-006
58,70	35120.4	140280	1.00E-006
72,78	252504	1007720	0.00E+000
80,86	370720	1480640	0.00E+000
97,100	33055.4	131990.6	1.00E-006
96,101	159530	635852	0.00E+000
103,108	22265.6	89065.2	2.00E-006
33,35	44303	176750	1.00E-006
48,51	62666.8	250208	1.00E-006
47,52	51189.6	204302	1.00E-006
46,53	92163.4	368424	1.00E-006
43,56	22265.6	88950.4	2.00E-006
45,54	31448.2	126252	1.00E-006
74,76	62666.8	250208	1.00E-006
73,77	92163.4	368424	1.00E-006

Table 3: Windkessel terminals corresponding to each arterial segment (for numbers see Table 2).

	Lower body			Upper body		
	Venules	Veins	Inferior cava	Venules	Veins	Superior cava
$R$ [dyn cm $^{-2}$ s ml $^{-1}$ ]	53.32	11.997	0.6665	186.62	39.99	0.6665
$L$ [dyn cm $^{-2}$ s $^2$ ml $^{-1}$ ]	1.333	0.6665	0.6665	1.333	0.6665	0.6665
$C$ [ml dyn $^{-1}$ cm $^2$ ]	0.00112528	0.05626407	0.01125281	0.00037509	0.01125281	0.00375094

Table 4: Data used in the 0D model of the venous circulation system.

Chambers	Right atrium	Right ventricle	Left atrium	Left ventricle
$E_A$ [dyn cm $^{-2}$ ml $^{-1}$ ]	79.98	733.15	93.31	3665.75
$E_B$ [dyn cm $^{-2}$ ml $^{-1}$ ]	93.31	66.65	119.97	106.64
$T_c$ [s]	0.17	0.34	0.17	0.34
$T_r$ [s]	0.17	0.15	0.17	0.15
$t_c$ [s]	0.80	—	0.80	—
$t_r$ [s]	0.97	—	0.97	—
$V_0$ [ml]	4.0	10.0	4.0	5.0
$\alpha$	0.0005	0.0005	0.0005	0.0005

Table 5: Data used in the elastance model of the right and left halves of the heart.

Valves	Tricuspid	Pulmonar	Mitral	Aortic
$R$ [dyn cm $^{-2}$ s ml $^{-1}$ ]	0.006	0.006	0.006	0.006
$L$ [dyn cm $^{-2}$ s $^2$ ml $^{-1}$ ]	0.005	0.005	0.005	0.005
$B$ [dyn cm $^{-2}$ s $^2$ ml $^{-2}$ ]	0.0064	0.00756	0.0064	0.00756
$\theta_{max}$ [°]	75.0	75.0	75.0	75.0
$\theta_{min}$ [°]	5.0	5.0	5.0	5.0
$k_P/I$ [rad s $^{-2}$ dyn $^{-1}$ cm $^2$ ]	4.126	4.126	4.126	4.126
$k_F/I$ [s $^{-1}$ ]	50.0	50.0	50.0	50.0
$k_Q/I$ [rad s $^{-1}$ ml $^{-1}$ ]	2.0	2.0	2.0	2.0
$k_V/I$ [rad s $^{-1}$ ml $^{-1}$ ]	3.5	3.5	3.5	7.0

Table 6: Data used in the non-ideal diode models of the cardiac valves.

	Pulmonary arteries	Pulmonary veins
$R$ [dyn cm $^{-2}$ s ml $^{-1}$ ]	106.64	13.33
$L$ [dyn cm $^{-2}$ s $^2$ ml $^{-1}$ ]	0.0	0.0
$C$ [ml dyn $^{-1}$ cm $^2$ ]	0.00309077	0.060015

Table 7: Data used in the 0D models for the compartments in the pulmonary circulation.

which the specific vessel is embedded. As for the values for the density and the viscosity of the blood, as with the 1D model, we take  $\rho = 1.04$  g/cm $^3$  and  $\mu = 0.04$  dyn s/cm $^2$ , respectively. When the Casson model is considered we set  $\mu_o = \mu$  and  $\tau_y = 0.038$  dyn/cm $^2$ .

## 4. Cardiovascular simulations

### 4.1. Numerical approximation

The numerical approximation of the model for the arterial tree network, eventually with an embedded 3D model, is carried out as in [4, 40]. The discretization of the 0D models is done following a second order Crank-Nicolson method combined with fixed point iterations for dealing with the non-differentiable non-linearity of the valve models.

### 4.2. Case 1: 1D-0D closed-loop model

In this first case we employ the 1D-0D closed-loop model (no 3D model is considered here). All the parameters for the standard case are those given in Section 3. Whenever a parameter is changed it is specified.

Figure 2 summarizes the results in several points throughout the cardiovascular system. These results are in accordance with patient-specific records published in the literature.

Figure 3 shows the flow rate and the opening angle in each one of the four cardiac valves. Observe that the dynamics is not described by a mere binary state. As well, as discussed in [21], the results given by this model

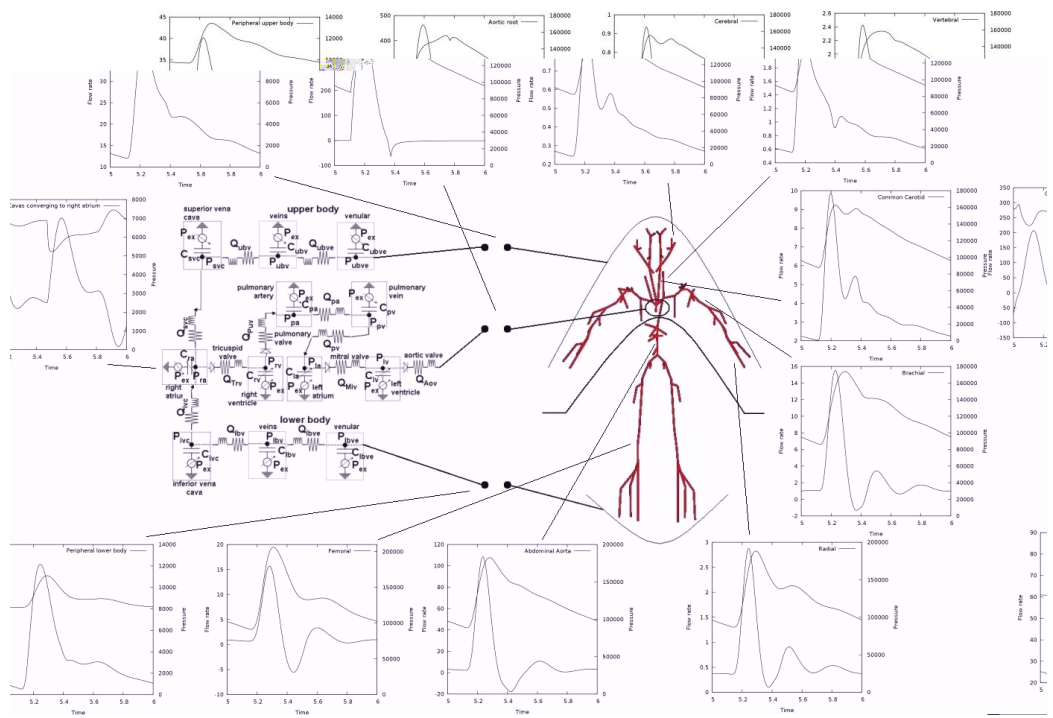


Figure 2: Results throughout the entire 1D-0D cardiovascular model.

with respect to the opening angle are in agreement with data reported in the literature concerning valve dynamics.

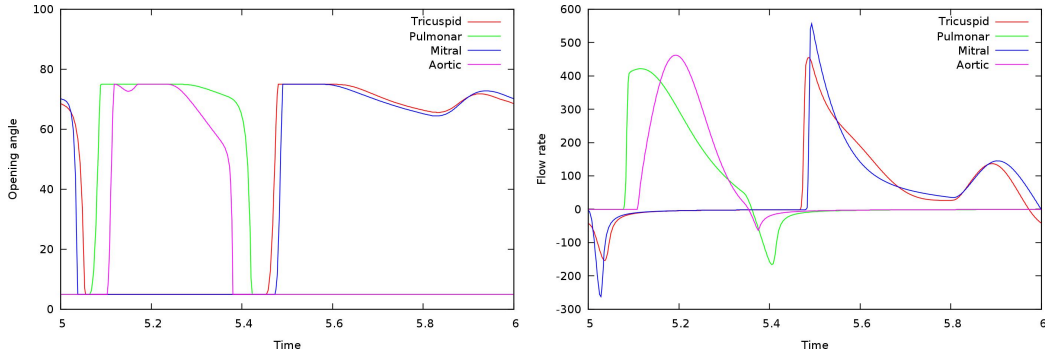


Figure 3: Opening angle and flow rate in the four cardiac valves.

In turn, Figure 4 displays the volume and the pressure in each cardiac chamber. It is worth saying that the present model is still under calibration using either data reported in the literature as well as patient-specific measurements in order to improve the results obtained from the simulations.

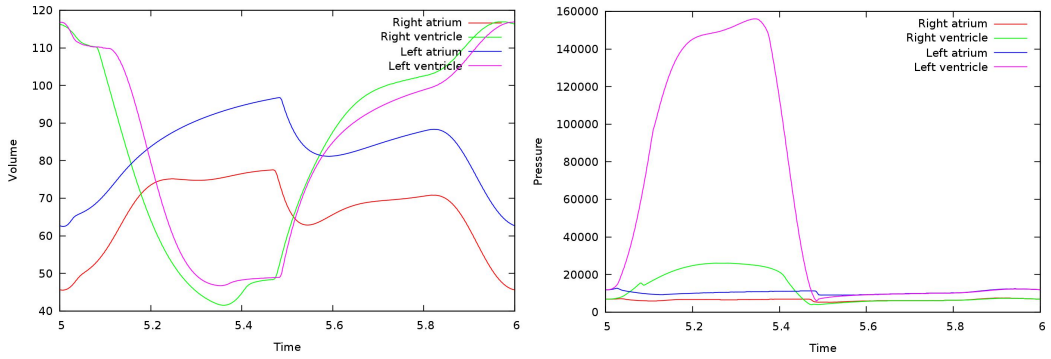


Figure 4: Volume and pressure in the four cardiac chambers.

Now we simulate the case in which we have a regurgitant aortic valve with different disease severities. The interested reader is referred to [21] for an exhaustive discussion on this topic, recalling that there the authors make use of a lumped model for the systemic arteries instead of the 128 arterial districts described by the 1D model used in the present work. We concentrate here on studying the sensitivity of the results when changing the severity of the disease. The regurgitant aortic valve is modelled by increasing

the minimum angle the valve is able to reach. The range tested here is  $\theta_{min,Aov} \in \{15^\circ, 20^\circ, 25^\circ, 30^\circ\}$  (see Table 6).

In all the simulations no auto-regulatory mechanism has been taken into account, noting that this is relevant for the correct description of the problem since the control mechanism play a main role in re-establishing the pressure to physiological values.

In Figures 5-8 we address the response of the system at several points. Figure 5 shows a notorious decrease in the left ventricle pressure during early systole, provoking the early opening of the aortic valve as seen also in that figure. In turn, the regurgitation in the aortic valve does not affect the dynamics of the mitral valve (opening angle) as shown in Figure 6. Nevertheless it affects the pressure in the right atrium, increasing its value.

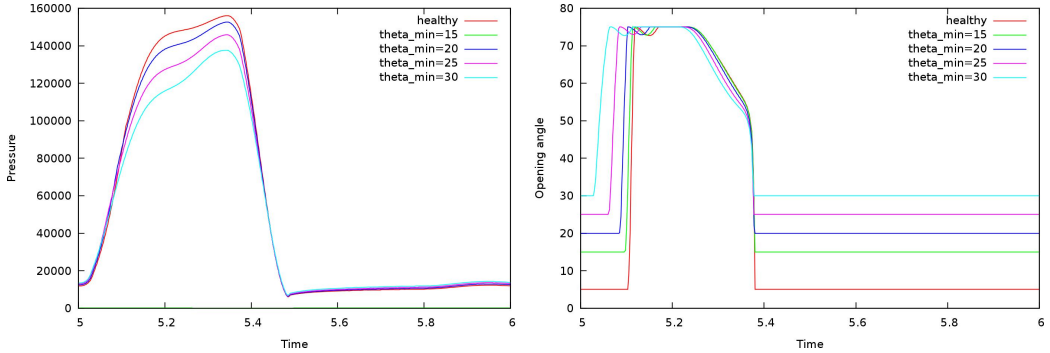


Figure 5: Comparison at the left ventricle between healthy and regurgitant aortic valve.

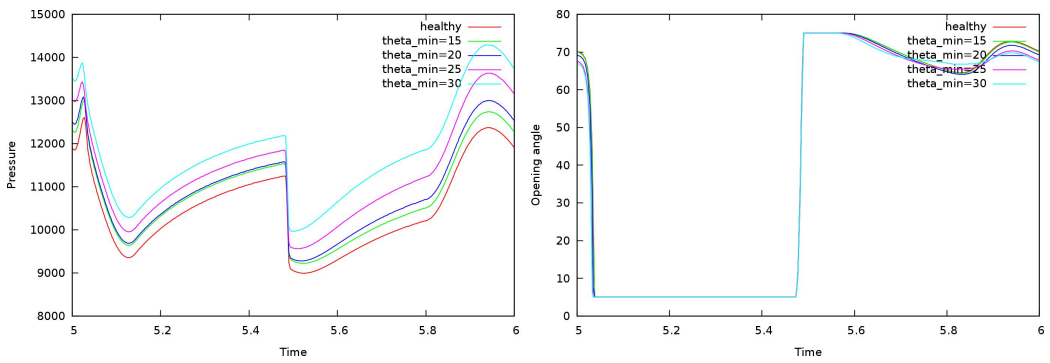


Figure 6: Comparison at the left atrium (and mitral valve) between healthy and regurgitant aortic valve.

Concerning the results in the systemic arteries (specifically at the aortic

root), Figures 7 and 8 present the flow rate and the pressure at the aortic root and at the common carotid artery, respectively. In Figure 7 the decrease in the diastolic pressure is significant, result of the valve insufficiency. Observe that the flow at the common carotid decreases to a point in which is becomes negative during diastole (due to the lack of auto-regulation in the system). Both figures also evince the decrease in the pressure during early systole, as with the pressure at the left ventricle. The lack of increase in the systolic pressure can be justified as a result of the lack for autoregulation in the cardiovascular system. It is easy to see that if such mechanisms are present, then they push the system back to a different homeostatic state with a higher pressure level. Now, since the systole-to-diastole pressure drop has been increased we would have an increased value of the pressure during systole and a decreased value during diastole.

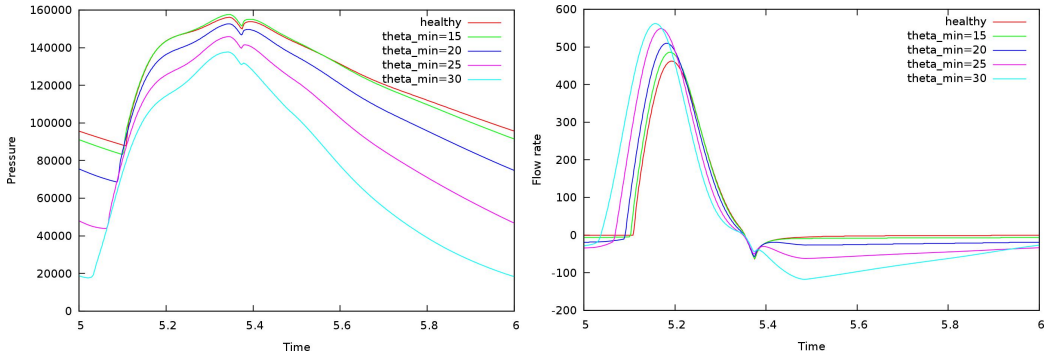


Figure 7: Comparison at the aortic root between healthy and regurgitant aortic valve.

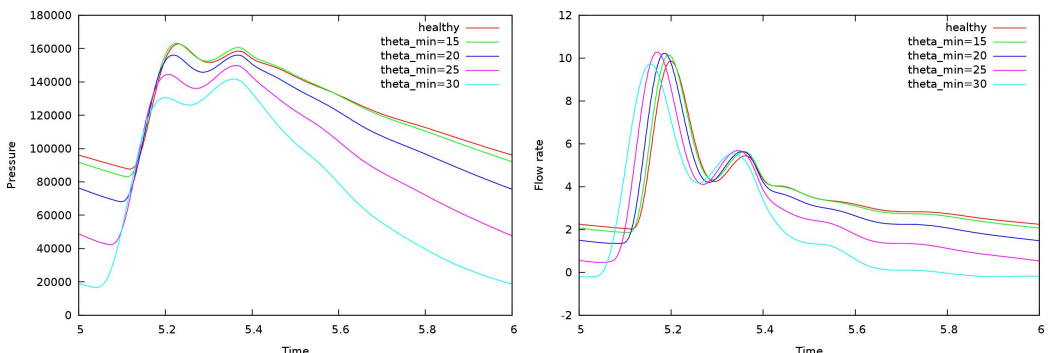


Figure 8: Comparison at the common carotid artery between healthy and regurgitant aortic valve.

The large sensitivity of the results observed in this example poses the question of whether homeostatic control mechanisms have to be incorporated in the model or not. Our results indicate that in situations like the one addressed here, in which the system has undergone strong alterations in its definition, it is compulsory to develop models to represent the short term control mechanisms in order to mediate the pressure in the cardiovascular system. This will certainly prevent an exaggerated drop pressure like the one observed in Figures 7-8. Some preliminary works have been developed [3], but more research in this direction is in order.

#### 4.3. Case 2: 3D-1D-0D closed-loop model

In this example we introduce a patient-specific cerebral aneurism into the 1D-0D closed-loop model for the cardiovascular system and perform simulations accounting for all the phenomena discussed in the preceding sections. Particularly, as in the previous example, we study the impact of the regurgitating aortic valve in the local hemodynamic environment of the cerebral aneurism. Schematically, we have the situation shown in Figure 9.

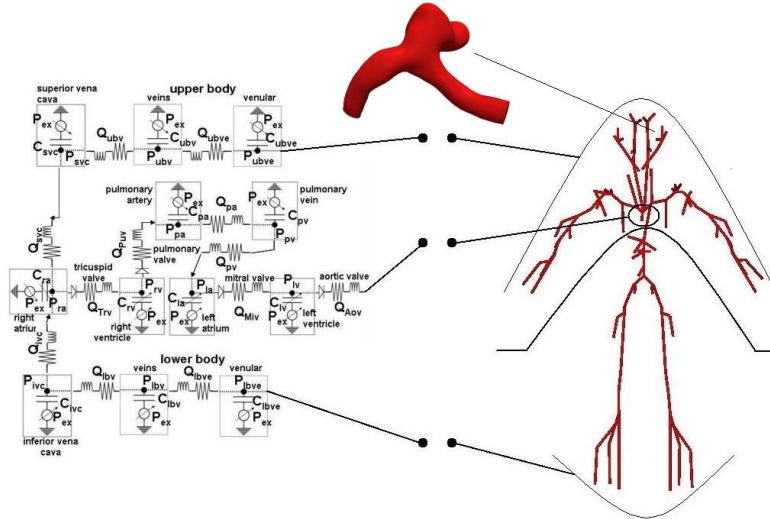


Figure 9: Scheme of the 1D-0D closed-loop model with a 3D patient-specific aneurism embedded in it.

The motivation to study this particular condition is the strong correlation between patients with infective endocarditis and rupture of mycotic aneurisms [10, 30, 35]. Most of the patients with acute aortic insufficiency

suffer from infective endocarditis, being this the cause of the valvular insufficiency due to bacteria attachment to the leaflets. In turn, patients with mycotic aneurisms suffering from infective endocarditis have a 60% of chances of aneurism rupture without warning. Therefore, the study of different hemodynamics conditions at a cerebral artery for different degrees of valve insufficiency may be of potential clinical interest.

Figure 10 presents the flow rate and the pressure at the proximal and distal coupling interfaces for the different degrees of pathological severity. First, notice the total inversion of the diastolic flow in the most acute case. Second, note the exaggerated drop in the pressure. These two facts should be revised with future research. Indeed, the drop pressure is not what we should expect in the sense that homeostatic control mechanisms should mediate the pressure, forcing the system in order to bring the pressure back to physiological values. This motivates further research in developing models for the control mechanisms acting over this 3D-1D-0D closed-loop model of the cardiovascular system.

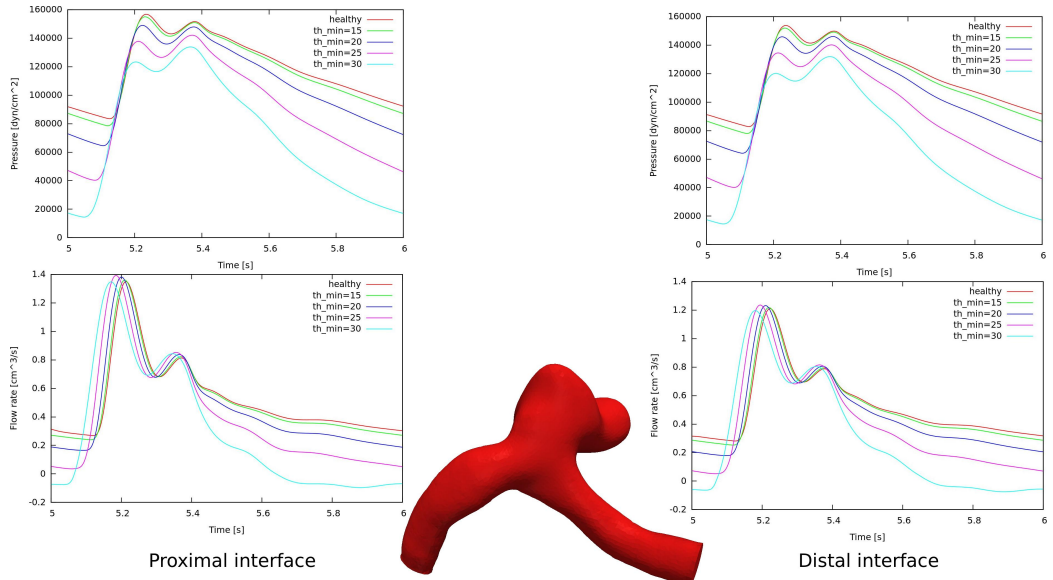


Figure 10: Pressure and flow rate at the proximal coupling interface.

To study of local hemodynamic quantities we will compute three quantities of interest: the wall shear stress index (WSS), the oscillatory shear index (OSI) and the mean residence time (MRT) (average of the residence time of

a set of particles released at the begining of the cardiac cycle).

In Figure 11 the WSS and the OSI indexes are presented for the five cases. The scales were accordingly changed in order to visualize the differences among the different scenarios. While the value of the WSS tends to be reduced with the development of the pathology into a more severe condition, the value of the OSI tends to increase. For the case  $\theta_{min} = 30$  the perspective was slightly changed to better notice the increase in the value of the OSI. This can be also observed in Table 8 where the averaged WSS and average OSI are presented. A substantial change in the value of the OSI occurs when the flow is completely inverted ( $\theta_{min} = 30$ ). This produces the oscillatory behavior of the stresses to take place not only in the intra-aneurismal region, but also in the parent artery.

To study the residence time a set of particles is released at the proximal location at the begining of the cardiac cycle. These trajectories are shown in Figure 12 for different time instants. In the detailed part of the figure, corresponding to a zoom in the intra-aneurismal volume all the trajectories are drawn together in order to compare the fluid dynamics in the different cases. Similarly to the variation of the WSS, the residence time of the particles decreases with the increase in the insufficiency severity. This can be seen in the MRT given in Table 8.

Case scenario	Avg WSS [dyn/cm <sup>2</sup> ]	Avg OSI	Avg MRT [s]
healthy	26.792	0.0138	0.170
$\theta_{min} = 15$	26.202	0.0142	0.152
$\theta_{min} = 20$	24.439	0.0150	0.137
$\theta_{min} = 25$	21.387	0.0169	0.128
$\theta_{min} = 30$	20.284	0.0664	0.112

Table 8: Averaged values of the WSS, OSI and MRT as a function of the aortic insufficiency severity.

It is worthwhile to point out that other hemodynamic quantities of interest could be computed as well as sensitivity analyses could be performed (see [7, 8, 9]). Our goal here was to motivate the use of this kind of models in order to understand the impact on the hemodynamics environment produced by changes in the global hemodynamics, within a context of arterial-venous-cardiac-pulmonary interaction. The sensitivity of the hemodynamics at this aneurism with respect to global factors is something that may help in answering questions about the influence of global variables, such as heart rate,

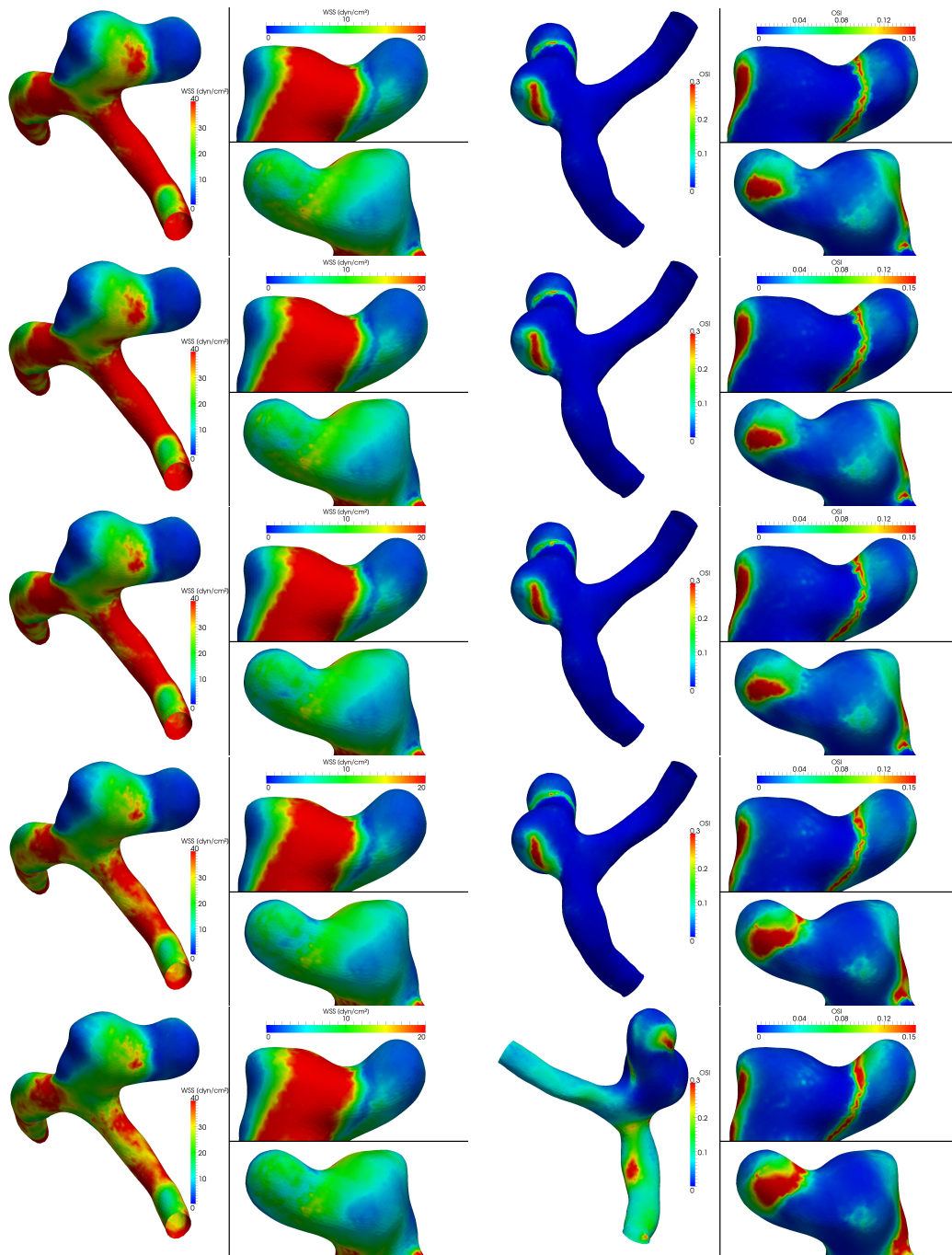


Figure 11: WSS and OSI indexes for the different degrees of insufficiency.

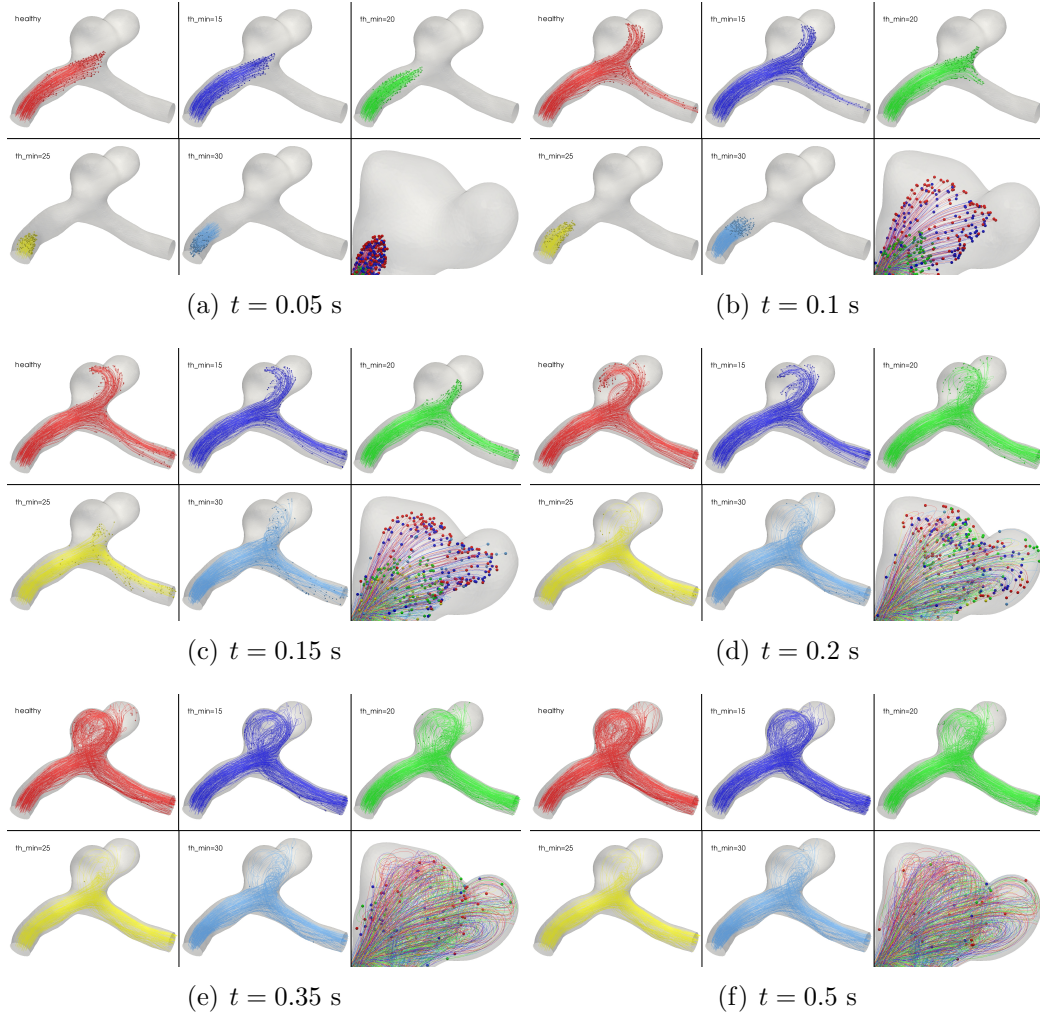


Figure 12: Particle trajectories at several time instants for different degrees of insufficiency. At each time instant from left to right and from top to bottom we have healthy (red),  $\theta_{min} = 15$  (blue),  $\theta_{min} = 20$  (green),  $\theta_{min} = 25$  (yellow),  $\theta_{min} = 30$  (light blue).

peripheral resistance, mean pressure, to local hemodynamics indexes which are believed to be connected with aneurysm rupture. No further comments are made here concerning this issue since this discussion is out of the scope of the present work.

Once again, it is important to notice the large sensitivity of the results with respect to the pathological conditions (see Table 8). As in the previous example, this dictates the need for incorporating control mechanisms in the system in order to study the cardiovascular response in a more physiological (or pathological as in this case) condition.

Indeed, several authors have recognized the need to integrate mathematical representations in order to create new models capable of addressing in a more realistic way the physical phenomena taking place in the cardiovascular system [16, 17, 34]. The results obtained here are consistent with this need, motivating further research in this field.

## 5. Final remarks

In this paper we have presented an integrative model of the cardiovascular system coupling different levels of detail for the blood circulation, ranging from the arterial/venous circulation to blood flow in specific vessels, accounting also for the peripheral circulation and non-ideal valve functioning.

This work comprises a step towards establishing a quite complex model which allows to analyze the interplay among several factors that render the closed-loop behavior of the cardiovascular system such as the arterial/venous coupling, the local/global hemodynamics and cardiac/arterial interactions, among others. With this kind of models it is truly possible to reproduce a wide range of physiological and pathophysiological scenarios being characterized by either global and local changes in the cardiovascular state.

A simple example of aortic valve regurgitation was addressed, and the sensitivity with respect to the insufficiency severity and its impact in terms of hemodynamics variables was briefly discussed. Furthermore, for these different degrees of aortic insufficiency 3D-1D-0D simulations were presented for the case of a patient-specific aneurism embedded in the 1D-0D closed-loop model for the cardiovascular system. Comparisons were presented in order to unveil the role of the global functioning of the closed-loop cardiovascular system and the local hemodynamic environment at the cerebral aneurism, which is believed to be related to the rupture phenomenon.

As well, from the discussions presented in this work, we conclude about the importance of incorporating to the present model short term homeostatic mechanisms, that is baroreflex, cardiopulmonary, chemoreflex and local controls. With this, it will be possible to consider the auto-regulation in the cardiovascular system whenever the sensitivity of the response as result of alterations in the definition of the system is large.

### Acknowledgements

This work was partially supported by the Brazilian agencies CNPq and FAPERJ. The support of these agencies is gratefully acknowledged.

### References

- [1] J. Alastruey, K.H. Parker, J. Peiró, S.M. Byrd, and S.J. Sherwin. Modelling the circle of Willis to assess the effects of anatomical variations and occlusions on cerebral flows. *J. Biomech.*, 40:1794–1805, 2007.
- [2] A.P. Avolio. Multi-branched model of the human arterial system. *Med. Biol. Engrg. Comp.*, 18:709–718, 1980.
- [3] P.J. Blanco, , and R.A. Feijóo. A dimensionally-heterogeneous model for the entire cardiovascular system integrated with a model of the autonomic nervous system. In *Proceedings of CMBE 2011. 2nd International Conference on Computational & Mathematical Biomedical Engineering, Nithiarasu et al. eds., Swansea, UK*, 2011.
- [4] P.J. Blanco, R.A. Feijóo, and S.A. Urquiza. A unified variational approach for coupling 3D-1D models and its blood flow applications. *Comp. Meth. Appl. Mech. Engrg.*, 196:4391–4410, 2007.
- [5] P.J. Blanco, M.R. Pivello, S.A. Urquiza, and R.A. Feijóo. On the potentialities of 3D–1D coupled models in hemodynamics simulations. *J. Biomech.*, 42:919–930, 2009.
- [6] P.J. Blanco, S.A. Urquiza, and R.A. Feijóo. Assessing the influence of heart rate in local hemodynamics through coupled 3D-1D-0D models. *Int. J. Num. Meth. Biomed. Engng.*, 26:890–903, 2010.

- [7] J.R. Cebral, M.A. Castro, S. Appanaboyina, C.M. Putman, D. Mil-lan, and A.F. Frangi. Efficient pipeline for image-based patient-specific analysis of cerebral aneurysm hemodynamics: technique and sensitivity. *IEEE Trans. Med. Imaging*, 24:457–467, 2005.
- [8] J.R. Cebral, F. Mut, J. Weir, and C.M. Putman. Association of hemo-dynamic characteristics and cerebral aneurysm rupture. *Am. J. Neuroradiol.*, 32:264–270, 2011.
- [9] J.R. Cebral, F. Mut, J. Weir, and C.M. Putman. Quantitative charac-terization of the hemodynamic environment in ruptured and unruptured brain aneurysms. *Am. J. Neuroradiol.*, 32:145–151, 2011.
- [10] P. Corr, M. Wright, and L.C. Handler. Endocarditis-related cerebral aneurysms: radiologic changes with treatment. *Am. J. Neuroradiol.*, 16:745–748, 1995.
- [11] L. Formaggia, J. F. Gerbeau, F. Nobile, and A. Quarteroni. On the cou-pling of 3D and 1D Navier-Stokes equations for flow problems in com-pliant vessels. *Comp. Meth. Appl. Mech. Engrg.*, 191:561–582, 2001.
- [12] L. Grinberg, T. Anor, J.R. Madsen, A. Yakhot, and G.E. Karniadakis. Large-scale simulation of the human arterial tree. *Clinical and Experi-mental Pharmacology and Physiology*, 36:194–205, 2009.
- [13] T. Heldt, E.B. Shim, R.D. Kamm, and R.G. Mark. Computational mod-eling of cardiovascular response to orthostatic stress. *J. Appl. Physiol.*, 92:1239–1254, 2002.
- [14] F.C. Hoppensteadt and C.S. Peskin. *Modeling and Simulation in Medicine and the Life Sciences*. Texts in Applied Mathematics, Springer, 2002.
- [15] T.J.R. Hughes. *A Study of the One-Dimensional Theory of Arterial Pulse Propagation*. PhD thesis, University of California, Berkeley, 1974.
- [16] J.D. Humphrey and C.A. Taylor. Intracranial and abdominal aortic aneurysms: similarities, differences, and need for a new class of computa-tional models. *Annu. Rev. Biomed. Engng.*, 10:221–246, 2008.

- [17] P. Hunter and P. Nielsen. A strategy for integrative computational physiology. *Physiology*, 20:316–325, 2005.
- [18] H.J. Kim, I.E. Vignon-Clementel, C.A. Figueroa, J.F. LaDisa, K.E. Jansen, J.A. Feinstein, and C.A. Taylor. On coupling a lumped parameter heart model and a three-dimensional finite element aorta model. *Ann. Biomed. Engng.*, 37:2153–2169, 2009.
- [19] Y. Kivity and R. Collins. Nonlinear fluid-shell interactions: application to blood flow in large arteries. *Int. Sym. Discrete Meth. Engrg.*, pages 476–488, 1974.
- [20] Y. Kivity and R. Collins. Nonlinear wave propagation in viscoelastic tubes: application to aortic rupture. *J. Biomech.*, pages 67–76, 1974.
- [21] T. Korakianitis and Y. Shi. Numerical simulation of cardiovascular dynamics with healthy and diseased heart valves. *J. Biomech.*, 39:1964–1982, 2006.
- [22] R.H. Kufahl and M.E. Clark. A circle of willis simulation using distensible vessels and pulsatile flow. *J. Biomech. Engrg.*, 107:112–122, 1985.
- [23] E. Lanzarone, P. Liani, and G. Baselli aand M.L. Constantino. Model of arterial tree and peripheral control for the study of physiological and assisted circulation. *Medical Engineering and Physics*, 29:542–555, 2007.
- [24] F. Liang and H. Liu. A closed-loop lumped parameter computational model for human cardiovascular system. *JSME International Journal*, 48:Series C, 2005.
- [25] F. Liang and H. Liu. Simulation of hemodynamic responses to the valsalva maneuver: An integrative computational model of the cardiovascular system and the autonomic nervous system. *J. Physiol. Sci.*, 56:45–65, 2006.
- [26] F. Liang and S. Takagi. Multi-scale modeling of the human cardiovascular system with applications to aortic valvular and arterial stenoses. *Med. Biol. Eng. Comput.*, 47:743–755, 2009.

- [27] F. Migliavacca, R. Balossino, G. Pennati, G. Dubini, T.-Y. Hsia, M.R. de Leval, and E.L. Bove. Multiscale modelling in biofluidynamics: Application to reconstructive paediatric cardiac surgery. *J. Biomech.*, 39:1010–1020, 2006.
- [28] M.S. Olufsen, J.T. Ottesen, H.T. Tran, L.M. Ellwein, L.A. Lipsitz, and V. Novak. Blood pressure and blood flow variation during postural change from sitting to standing: model development and validation. *J. Appl. Physiol.*, 99:1523–1537, 2005.
- [29] M.S. Olufsen, C.S. Peskin, W.Y. Kim, E.M. Pedersen, A. Nadim, and J. Larsen. Numerical simulation and experimental validation of blood flow in arteries with structured-tree outflow conditions. *Ann. Biomed. Engng.*, 28:1281–1299, 2000.
- [30] S.M. Oppenheimer and J. Lima. Review: Neurology in medicine. neurology and the heart. *J. Neurol. Neurosurg. Psychiatry*, 64:289–297, 1998.
- [31] G. Pontrelli. A multiscale approach for modelling wave propagation in an arterial segment. *Comp. Meth. Biomech. Biom. Engrg.*, 7:79–89, 2004.
- [32] J. Reichold, M. Stampanoni, A.L. Keller, A. Buck, P. Jenny, and B. Weber. Vascular graph model to simulate the cerebral blood flow in realistic vascular networks. *J. Cereb. Blood Flow Metab.*, 29:1429–1443, 2009.
- [33] P. Reymond, F. Merenda, F. Perren, D. Rüfenacht, and Nikos Stergiopoulos. Validation of a one-dimensional model of the systemic arterial tree. *Am. J. Physiol. Heart Circ. Physiol.*, 297:H208–H222, 2009.
- [34] J.J. Ricotta, J. Pagan, M. Xenos, Y. Alemum, S. Einav, and D. Bluestein. Cardiovascular disease management: the need for better diagnostics. *Med. Biol. Engng. Comput.*, 46:1059–1068, 2008.
- [35] A.V. Salgado, A.J. Furlan, and T.F. Keys. Mycotic aneurysm, subarachnoid hemorrhage, and indications for cerebral angiography in infective endocarditis. *Stroke*, 18:1057–1060, 1987.

- [36] B.W. Schaaf and P.H. Abbrecht. Digital computer simulation of systemic arterial pulse wave transmission: a nonlinear model. *J. Biomech. Engrg.*, 5:345–364, 1972.
- [37] M.P. Spencer and A.B. Deninson. The square-wave electro-magnetic flowmeter. Theory of operation and design of magnetic probes for clinical and experimental applications. *I.R.E. Trans. Med. Elect.*, 6:220–228, 1959.
- [38] N. Stergiopoulos, D.F. Young, and T.R. Rogge. Computer simulation of arterial flow with applications to arterial and aortic stenoses. *J. Biomech.*, 25:1477–1488, 1992.
- [39] J.C. Stettler, P. Niederer, and M. Anliker. Theoretical analysis of arterial hemodynamics including the influence of bifurcations, part I. *Ann. Biomed. Engrg.*, 9:145–164, 1981.
- [40] S.A. Urquiza, P.J. Blanco, M.J. Vénere, and R.A. Feijóo. Multidimensional modeling for the carotid blood flow. *Comp. Meth. Appl. Mech. Engrg.*, 195:4002–4017, 2006.
- [41] K. van Heusden, J. Gisolf, W.J. Stok, S. Dijkstra, and J. M. Karemaker. Mathematical modeling of gravitational effects on the circulation: importance of the time course of venous pooling and blood volume changes in the lungs. *Am J. Physiol. Heart Circ. Physiol.*, 291:H2152–H2165, 2006.
- [42] I.E. Vignon-Clementel, C.A. Figueiroa, K.E. Jansen, and C.A. Taylor. Outflow boundary conditions for three-dimensional finite element modeling of blood flow and pressure waves in arteries. *Comp. Meth. Appl. Mech. Engrg.*, 195:3776–3996, 2006.
- [43] J.J. Wang and K.H. Parker. Wave propagation in a model of the arterial circulation. *J. Biomech.*, 37:457–470, 2004.